ADVANCED FUNCTIONAL MATERIALS
www.afm-journal.de

Reducing Surface Roughness to Achieve Li_2CO_3-Existent Lithiophilic Interface in Garnet-Type Solid-State Batteries

Jiaxu Zhang, Changhong Wang, Jiamin Fu, Minghao Ye, Huiyu Zhai, Jun Li, Gangjian Tan, Xinfeng Tang,* and Xueliang Sun**

The presence of Li_2CO_3 has been identified as the cause of poor lithophilicity in garnet-type $Li_7La_3Zr_2O_{12}$ (LLZO) solid-state batteries. A Li_2CO_3-free garnet is expected to enhance the Li/LLZO interface contact. However, permanently eradicating regenerative Li_2CO_3 from the LLZO surface is extremely challenging and the influence of regenerated Li_2CO_3 is often ignored. Herein, it is found that glossy Li_2CO_3 pellets can also be perfectly wetted by molten Li, contradicting the common belief that Li_2CO_3 is lithiophobic. Therefore, reducing the surface roughness of LLZO allows it to be directly wetted by lithium metal, regardless of the presence of Li_2CO_3. Additionally, smooth LLZO exhibits better air stability due to its reduced active area. The symmetric cell with a smooth LLZO pellet shows a low interfacial impedance of 2 Ω cm^2 and a high critical current density of 1.4 mA cm^{-2} at 25 °C. This work highlights the surface physics of garnet which significantly influences its interface properties, apart from surface chemistry.

1. Introduction

Lithium-ion batteries (LIBs) have garnered significant interest in the energy storage sector due to their long cycle life and high energy density. However, conventional LIBs with liquid organic electrolytes pose inherent safety risks.[1–3] Solid-state electrolytes (SSEs) show promise as substitutes for the liquid organic electrolytes in LIBs, offering a potential solution to these safety risks.[4] Additionally, the resistance of SSEs to lithium dendrites enables compatibility with high-capacity lithium metals (3860 mAh g^{-1}), substantially enhancing the energy density in all-solid-state lithium batteries (ASSLBs).[5] Under this circumstance, various SSEs have been developed in the past decades, including oxide,[6–8] sulfide,[9–11] halide,[12–14] polymer,[15–17] and composite electrolytes.[18–20] $Li_7La_3Zr_2O_{12}$ (LLZO), a garnet-type oxide electrolyte, stands out as a promising SSE for ASSLBs owing to its high Li-ion conductivity at room temperature, good electrochemical stability with lithium metal, and wide electrochemical window.[21,22] However, garnet-type oxide electrolyte pellets usually exhibit poor wettability with lithium metal, leading to substantial interfacial resistance and non-uniform ion transport across the interface.[23,24]

In general, the surface chemical property of LLZO highly influences lithium wettability. It is well known that Li_2CO_3 spontaneously generates on the surface when exposed to air, which greatly reduces the lithium wettability.[25] To address the issue, many strategies have been proposed. For example, directly coating lithiophilic materials on the LLZO surface to achieve a tight Li/LLZO interface without removing surface Li_2CO_3.[26–29] The actual interfacial structure can be equivalent to "LLZO/Li_2CO_3/lithiophilic layer/Li". In addition, directly converting the Li_2CO_3 layer into a lithiophilic layer is another approach to improve the wettability of garnet. For instance, NH_4F treatment was applied to convert the Li_2CO_3 into a fluorinated lithiophilic interface.[30] In this case, the wetted interface can be simplified as "LLZTO/lithiophilic layer/Li". Furthermore, removing Li_2CO_3 from the LLZO surface has also been attempted by chemical corrosion[31] or physical cleaning,[32,33] which is deemed to expose the lithiophilic bare LLZO to lithium metal and get a tight "LLZO/Li" interface. However, it is still challenging to get an absolute Li_2CO_3-free surface for the garnet because of the regenerative nature of Li_2CO_3 even in an inert

J. Zhang, M. Ye, H. Zhai, J. Li, G. Tan, X. Tang
State Key Laboratory of Advanced Technology for Materials Synthesis and Processing
Wuhan University of Technology
Wuhan 430070, China
E-mail: gtan@whut.edu.cn; tangxf@whut.edu.cn
J. Zhang, C. Wang, X. Sun
Ningbo Key Laboratory of All-Solid-State Battery
Eastern Institute for Advanced Study
Eastern Institute of Technology
Ningbo 315200, China
E-mail: xsun9@uwo.ca
J. Zhang
School of Chemistry and Materials Science
University of Science and Technology of China
Hefei 230026, China
J. Fu
Department of Mechanical and Materials Engineering
University of Western Ontario
1151 Richmond St., London, Ontario N6A 3K7, Canada

The ORCID identification number(s) for the author(s) of this article can be found under https://doi.org/10.1002/adfm.202416229

DOI: 10.1002/adfm.202416229

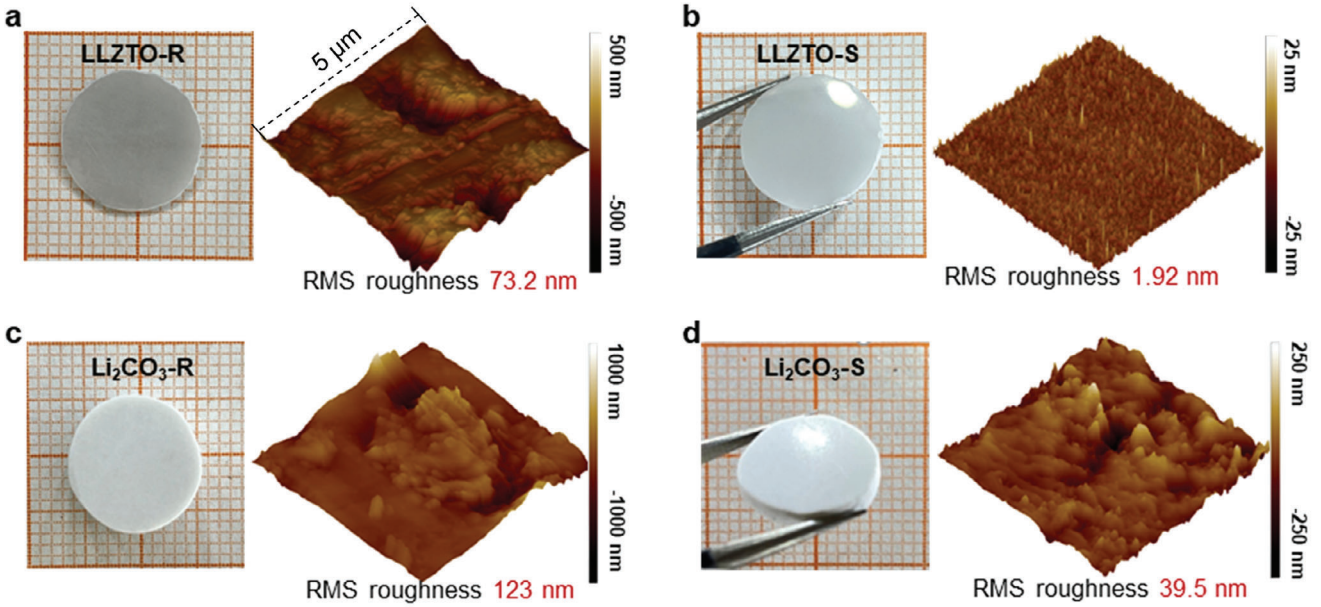

Figure 1. a) Optical images and AFM scans (5 × 5 μm) of the LLZTO-R pellet surfaces. b) Optical images and AFM scans of the LLZTO-S pellet surfaces. c) Optical images and AFM scans of the Li_2CO_3-R pellet surfaces. d) Optical images and AFM scans of the Li_2CO_3-S pellet surfaces.

atmosphere.[34,35] Therefore, seeking new strategies to achieve a tight Li/LLZO interface without removing Li_2CO_3 is still needed.

In this work, we developed a feasible approach to effectively achieve a tight Li/LLZO interface by reducing the surface roughness of LLZO. By preparing a series of LLZO and bare Li_2CO_3 pellets with different surface roughness via hot-pressing and plasma sintering, the relationship between surface roughness and lithiophility is qualitatively decoupled. We investigate the wetting behaviors of Li metal on LLZO pellets under different surface roughness. It is found that the LLZO pellet with low surface roughness can be easily wetted by lithium metal without removing surface Li_2CO_3, which implies the Li_2CO_3 can be lithiophilic as long as keeping low surface roughness. In addition, the LLZO pellet with low surface roughness displays better air stability, which is attributed to the smaller specific surface area. At last, without importing an intermediate layer or changing the surface chemistry of garnet, the symmetric cell assembled with the smooth LLZO pellet displays a low interfacial impedance (2 Ω cm^2) and a high critical current density (CCD) of 1.4 mA cm^{-2} at 25 °C. These encouraging results and the finding of "lithiophilic Li_2CO_3" may represent one of the most critical understandings in garnet-type ASSBs.

2. Results and Discussion

2.1. Apparent and Microscopic Morphology

The Ta-doped cubic garnet-type electrolyte powder $Li_{6.4}La_3Zr_{1.4}Ta_{0.6}O_{12}$ (denoted as LLZTO hereafter) is densified by hot pressing for 1 h at 1150 °C under an axial pressure of 20 MPa in Ar atmosphere. The densified pellets were then polished with sandpaper and polisher with different polishing abrasives (details in the Supporting Information). The atomic force microscopy (AFM) was applied to characterize the morphology of these pellets (**Figure 1**; Figure S1, Supporting Information). As shown in Figure 1a,c, the LLZTO pellet and Li_2CO_3 pellet polished with 2000 grit SiC abrasive paper (denoted as LLZTO-R and Li_2CO_3-R) displays a macroscopic rough surface with visible scratch, which displays the root-mean-square (RMS) roughness of 73.2 and 123 nm, respectively. In contrast, the LLZTO pellet and Li_2CO_3 pellet polished with 0.05 μm abrasives (denoted as LLZTO-S and Li_2CO_3-S) display a macroscopic smooth surface, Figure 1b,d. The surface RMS roughness of LLZTO-S and Li_2CO_3-S is 1.92 and 39.5 nm, respectively. These results confirm that the simple polishing methods can effectively reduce the surface roughness of the LLZTO or Li_2CO_3 pellets. The reduction of roughness is to some extent controllable, which is convenient for studying the relationship between the roughness and wettability of LLZTO pellet. In addition, the temperature dependent EIS measurement (Figure S10, Supporting Information) performed on LLZTO pellet indicates an ionic conductivity of 5.9 × 10^{-4} S cm^{-1} at 25 °C and activation energy of 0.299 eV. The electronic conductivity was determined to be 6.82 × 10^{-8} and 6.59 × 10^{-8} S cm^{-1} for the LLZTO-S and LLZTO-R, respectively. (Figure S9, Supporting Information) The testing results agree well with previous studies.[49]

2.2. Surface Chemical Property and Air-Stability Analysis

In situ X-ray photoelectron spectroscopy (XPS) measurement was conducted on the LLZTO-S and LLZTO-R pellet surface. The two pellets were prepared and then were immediately transferred to the high vacuum XPS chamber. As shown in **Figure 2a**, the C 1s spectrum for LLZTO-S displays a strong peak at the

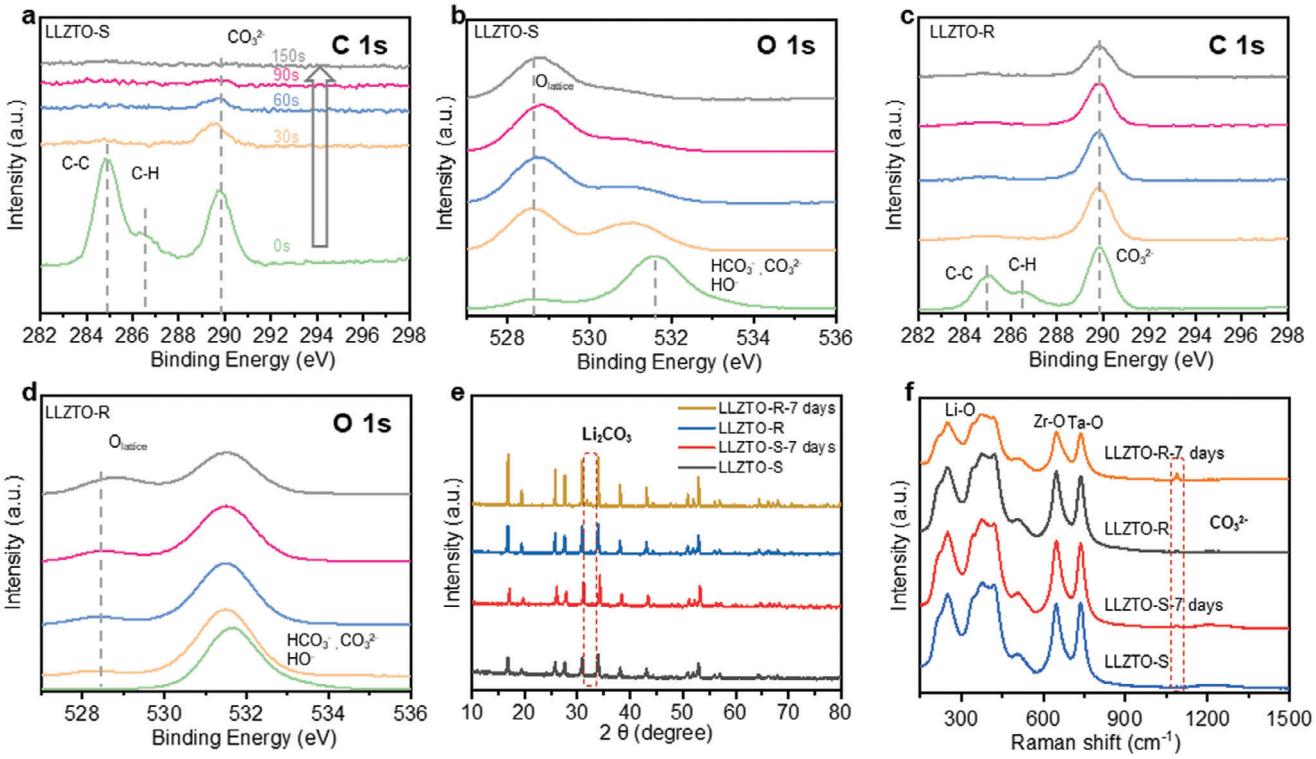

Figure 2. Surface chemical property and air-stability analysis. a) C 1s, and b) O 1s XPS data collected from LLZTO-S pellet original surface and after 30, 60, 90, and 150 s of Ar^+ ion sputtering. c) C 1s, and d) O 1s XPS data collected from LLZTO-R pellet original surface and after 30, 60, 90, and 150 s of Ar^+ ion sputtering. e) XRD patterns were collected from LLZTO-S and LLZTO-R pellets and after exposed them in air for a week. f) Raman spectra were collected from LLZTO-S and LLZTO-R pellets and after exposed them in air for a week.

binding energy of 290 eV corresponding to CO_3^{2-}, which indicates the presence of carbonate species on the LLZTO-S surface. The peaks at 285 associated with C–C species are primarily from the adventitious carbon.[36] After etching by Ar ion for 30 s, most of the adventitious carbon was removed, and the peaks vanished. With the etching time increase to 150 s, the peaks at 290 eV correlate with CO_3^{2-} also vanished. This indicated the Li_2CO_3 layer on the surface of LLZTO-S was removed. In addition, as the increase of etching time, the intensity of the peak at 531.7 eV associated with carbonate species decreases, and the intensity of the peaks ≈528.5 eV related to the lattice oxygen in LLZTO increases,[37,38] Figure 2b. This also indicates the removal of the Li_2CO_3 layer. In contrast, after etching by 150 s, the peak located at 290 and 531.7 eV still displays high intensity for LLZTO-R, Figure 2c,d, which signifies the much thicker Li_2CO_3 layer in LLZTO-R. Theoretically, the Li_2CO_3 on the surface of the pellet has been removed because the garnet pellets were fully polished. Li_2CO_3 quickly forms again when the surface Li_2CO_3-free pellets are re-exposed to air during transfer to the XPS chamber.[33] Hence, XPS analysis with Ar^+ etching confirmed that the Li_2CO_3 layer was thinner for LLZTO-S than that of LLZTO-R, indicating the improved air stability of LLZTO-S. X-ray diffraction and Raman spectra were employed to confirm the air stability for LLZTO-S. As shown in Figure 2e, we employed X-ray diffraction to detect the phase information of the freshly prepared LLZTO-S and LLZTO-R pellets. And they are in agreement with the cubic structured $Li_5La_3Nb_2O_{12}$ (PDF # 80–0457). Both LLZTO-S and LLZTO-R pellets were exposed at a temperature of 30 °C and a humidity of 60% in air for a week, followed by XRD tests. As speculated above, evident peaks at 32° associated with lithium carbonate emerged for LLZTO-R pellet, which revealed the generation of Li_2CO_3 species after air exposure. However, the intensity of the peaks associated with lithium carbonate for LLZTO-S pellet is lower. Several characteristic peaks related to cubic garnet are recorded in Raman spectra for both samples, Figure 2e. And no obvious peak related to Li_2CO_3 was detected for the freshly prepared LLZTO-S and LLZTO-R pellets.[39] After exposed in air, a strong peak related to Li_2CO_3 at 1090 cm^{-1} emerged for LLZTO-R pellets, while a weaker peak appeared in LLZTO-S.[40] The stronger peak further indicated much more Li_2CO_3 was generated on the LLZTO-R surface than that on the LLZTO-S surface. Moreover, we measured the ionic conductivity of LLZTO-R and LLZTO-S before and after a week of air exposure (Figure S8, Supporting Information). The LLZTO-R and LLZTO-S displays the ionic conductivity of 6.1×10^{-4} and 5.9×10^{-4} S cm^{-1}, respectively. After being exposed to air for a week, the ion conductivity of LLZTO-S remained the same (5.7×10^{-4} S cm^{-1}), but the LLZTO-R displays a slightly reduced ion conductivity (5.5×10^{-4} S cm^{-1}) due to the generate thick Li_2CO_3 layer. Hence, LLZTO-S displays better air stability than LLZTO-R. We conclude that LLZTO-S has a lower actual specific surface area, which means a less reactive active site. Hence, compared with LLZTO-R, LLZTO-S

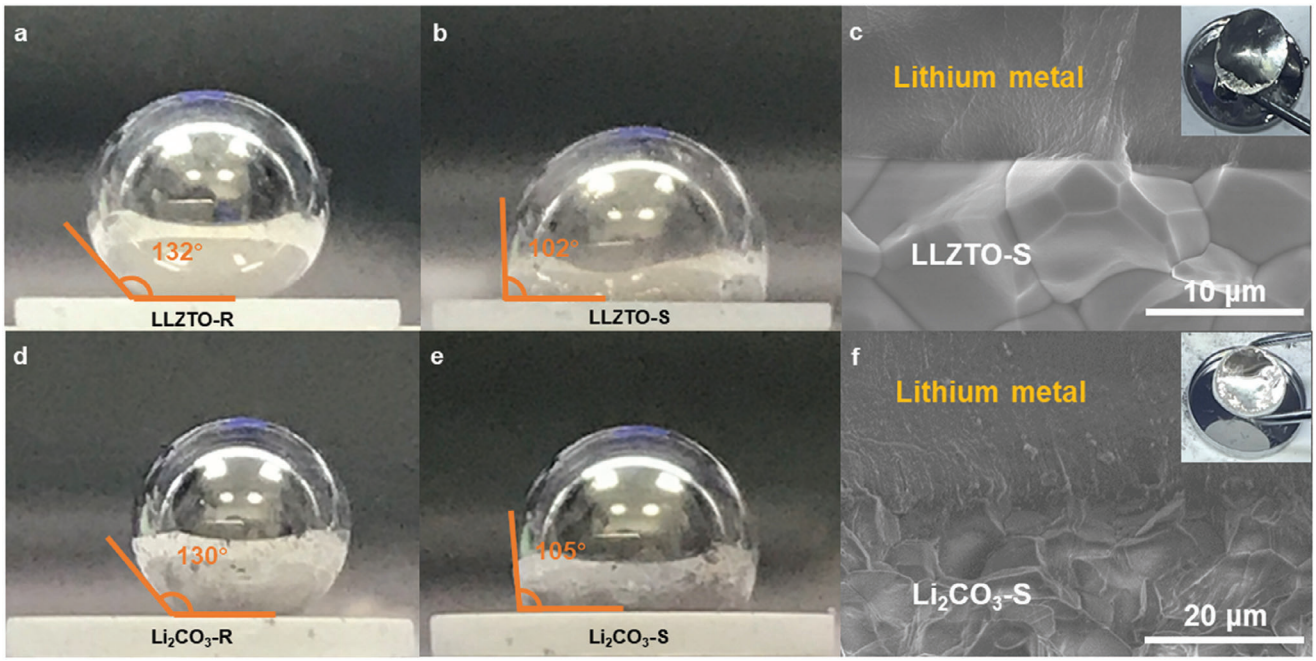

Figure 3. a) Contact angle of molten Li metal on LLZTO-R pellet. b) Contact angle of molten Li metal on LLZTO-S pellet. c) SEM images of interfaces between Li metal and LLZTO-S pellet. The wetting behavior between molten Li metal and LLZTO@-S pellet was shown in the inset of c). d) Contact angle of molten Li metal on Li_2CO_3-R pellet. e) Contact angle of molten Li metal on Li_2CO_3-S pellet. f) SEM images of interfaces between Li metal and Li_2CO_3-S pellet. The wetting behavior between molten Li metal and Li_2CO_3-S pellet was shown in the inset of (f).

displays a lower reaction rate to moist air. Nanoscope analysis was used to fit the actual surface area of the pellets (obtained from 5 × 5 μm AFM images). As shown in Figure S2 (Supporting Information), the actual surface area of the pellets increases with the increase of the RMS roughness. And the LLZTO-S and LLZTO-R display the actual surface of 25.17 and 28 μm respectively.

2.3. The Relationship Between Surface Roughness and Interface Wettability for Pellet

To characterize wettability, the contact angle of molten lithium metals on the LLZTO pellet with different surface roughness was measured. As shown in Figure S3 (Supporting Information), with the decreasing of RMS roughness, the LLZTO pellet can be easily wetted by molten lithium metal. And the corresponding contact angle between the LLZTO and lithium metal also decreases, Figure S4 (Supporting Information). Take the LLZTO-S and LLZTO-R for example, as shown in **Figure 3**a,b, the LLZTO-R displays a contact angle of 132°, but the LLZTO-S exhibited a lower contact angle of 102°. This indicates the wettability of the LLZTO pellet is improved. As a result, when pressing the pellet into the molten lithium with tweezers and rubbing it for a few seconds, the LLZTO-S displays great wettability with molten lithium. The interfacial contact between LLZTO-S and lithium metal becomes tight and there are no obvious gaps under the observation of scanning electron microscopy (SEM), Figure 3c. In addition, X-ray computed tomography (XCT) is carried out to image the Li/LLZTO-S interface. As shown in Figure S11a,b (Supporting Information), there are no obvious gaps under the XCT scans. Interestingly, it is normally reported that the Li_2CO_3 is naturally lithiophobic. As shown in Figure 3d, the densified Li_2CO_3 pellet polished by 2000 grit sandpaper cannot be wetted by the molten lithium metal, which exhibited a high contact angle of 136°. However, we find that the polished Li_2CO_3 can be lithiophilic. As shown in Figure 3e, the polished Li_2CO_3 pellet with a roughness of 39.5 nm can be well wetted by lithium metal, which exhibited a low contact angle of 105°. As shown in Figure 3f and Figure S12 (Supporting Information), the polished Li_2CO_3 pellet also displays good wettability when pressed into the molten lithium with tweezers. (Video S1, Supporting Information, ESI†) Under the observation of the SEM, the Li/Li_2CO_3 interface is also seamless which is similar to the Li/LLZTO-S interface. Additionally, XCT further confirms the seamless interface of the Li/Li_2CO_3, Figure S11c,d, Supporting Information). This abnormal phenomenon can be explained by Wenzel's theory[41]: For a hydrophobic surface, the smoother it is, the more hydrophilic it can be. The corresponding equation is

$$\mathrm{Cos}\ \theta_r = f\mathrm{Cos}\theta_s \quad (1)$$

where θ_r means the contact angle of liquid on the actual roughness surface, f stands for the actual area divided by the ideal area. θ_r refer to the contact angle of liquid on the ideal smooth surface. As shown in Figure S5 (Supporting Information), we tested the contact angle between the pellets with different roughness and molten lithium metal. The dates obtained from Nanoscope show that the surface actual area is in direct proportion to the f. The f is also in direct proportion to the contact angle, which corresponds to the Equation (1).

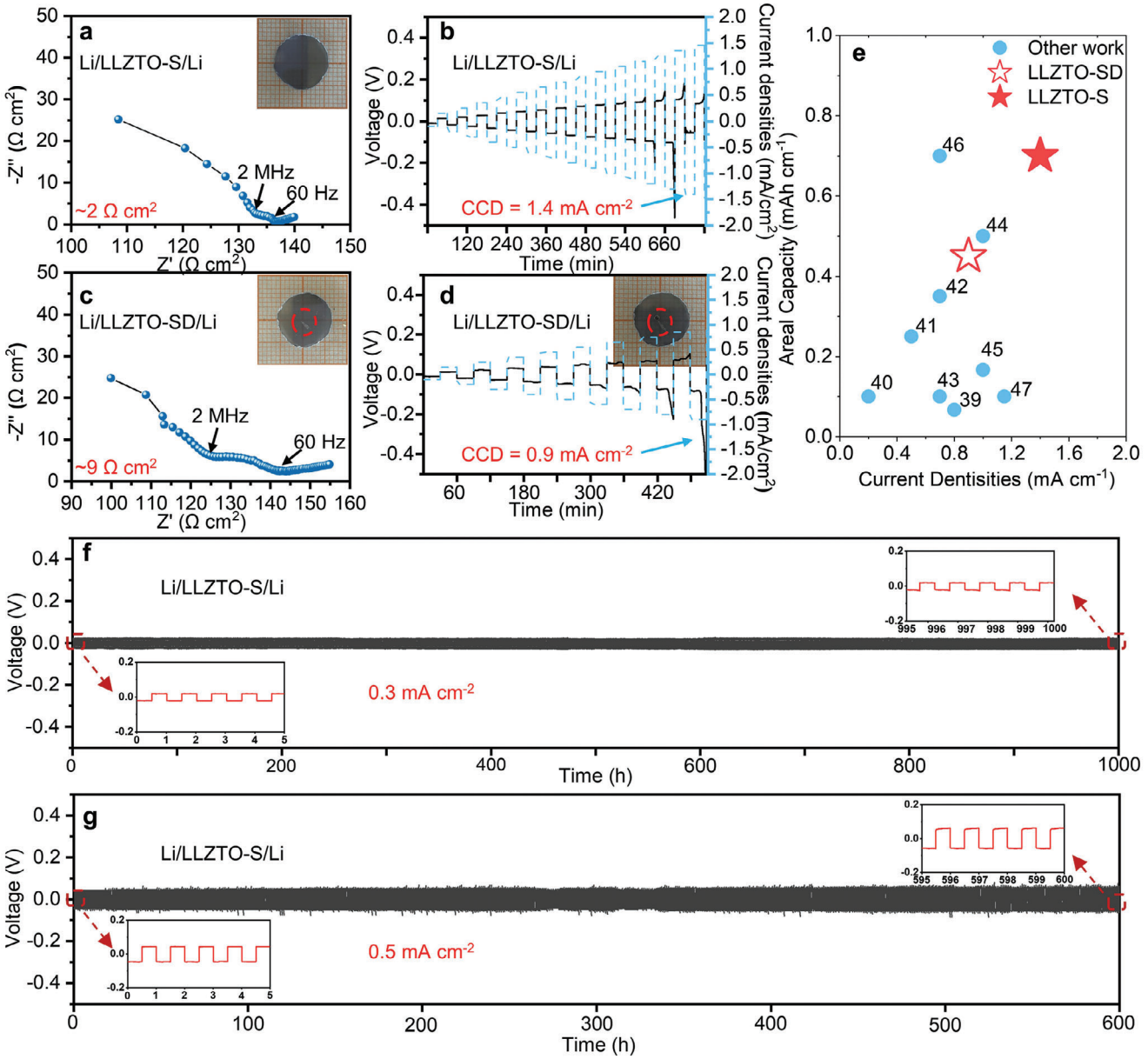

Figure 4. Electrochemical characterization of the symmetric cells. a) EIS measurements of the Li/LLZTO-S/Li symmetric cells. b) Polarization curve of the symmetric cell at different current densities (30 min for per plating or stripping). c) EIS measurements of the Li/LLZTO-SD/Li symmetric cells. d) Polarization curve of the symmetric cell at different current densities (30 min for per plating or stripping). e) Comparison of CCD of Li–Li symmetric cells. (f, g) Polarization curve of Li/LLZTO-S/Li symmetric cell during the long-term striping-plating process (1 h for a per-cycle) at a current density of f) 0.3, and g) 0.5 mA cm^{-2}. Insets show the magnifying curves at different times during the cycle process.

2.4. Demonstration of Excellent Electrochemical Performance in Assembled Batteries

Li symmetric cells were assembled and tested to confirm the positive effects of reducing the surface roughness on the electrochemical performance. EIS was conducted to demonstrate the interfacial impedance, as shown in Figure S6 (Supporting Information), the total resistance is ≈439 ohm cm^2 for the Li/LLZTO-R/Li cell. The resistance from the garnet bulk is the partial semicircle at high frequency, which is ≈111 ohm cm^2. Hence, after subtracting the garnet bulk resistance from the total resistance, the interfacial resistance is calculated to be ≈164 ohm cm^2. With the same calculating method, the interfacial resistance for Li/LLZTO-S/Li symmetric cell is estimated to be ≈2 Ohm cm^2, **Figure** 4a. The critical current density (CCD) of Li/LLZTO-S/Li symmetric cell was also tested under step-increased current densities. As shown in Figure 4b, it is seen that the Li/LLZTO-S/Li cell maintains work until a CCD of 1.4 mA cm^{-2}. The large CCD in Li/LLZTO-S/Li symmetric cell indicates the tight and stable Li/LLZTO interface was achieved by smoothing the garnet surface. To further confirm the advantages of the smooth surface, we destroy the smooth surface of

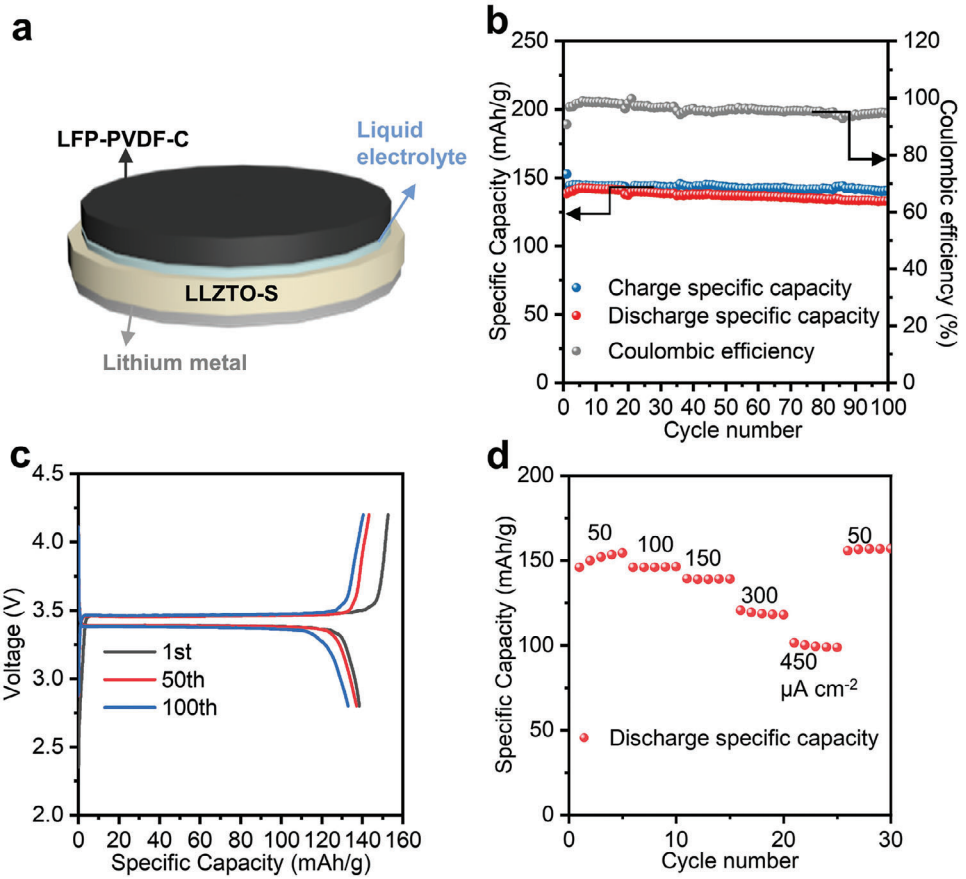

Figure 5. a) Schematic of the full cell with LFP cathode, LLZTO-S electrolyte, and Li anode. b) Cycling performance of the LFP/LLZO/Li cell at a current density of 30 μA cm^{-2}. c) Charge/discharge curves of LFP/LLZO/Li cell at different cycles. d) Rate performance of the full cell at different current densities.

LLZTO-S with a diamond-tipped tool intentionally (denoted as LLZTO-SD), which is marked by the red line in Figure 4c. As a result, the interface resistance of Li/LLZTO-SD/Li increased, which is calculated to be ≈9 ohm cm^2. In addition, the assembled symmetric cell displays a decreased CCD of 0.9 mA cm^{-2}, Figure 4d. The symmetric cell was disassembled after breakdown and the lithium metal electrode was separated carefully from LLZTO-SD. Interestingly, cracks formed and extended near the scratched area, which was observed by the optical camera, Figure 4d. The pellet was cut at this area and further observed under cross-section SEM as shown in Figure S7 (Supporting Information), where the lithium dendrites were confirmed. From a thermodynamic perspective, the microstructure of a solid surface affects its affinity to the liquid.[42,43] Molten lithium metal exhibits varying affinity when in contact with LLZO, because the surface energy depends on the surface microstructure.[44] Herein, the molten lithium shows poor affinity to the damaged LLZTO surface, which leads to a weak solid-solid interface and the formation of pores. Hence, inhomogeneous Li^+ flux occurs during Li stripping/plating, which will accelerate the formation Li dendrites.[45] The Li plating/striping areal capacity was calculated from the CCD data (Figure 4b,d) and compared to the performance of other work,[46–54] as shown in Figure 4e. The Li/LLZTO-S/Li cell showed outstanding performance compared to other reported results.

The prolonged stability during the lithium striping and plating for the Li/LLZTO-S/Li symmetric cell is tested at the current densities of 0.3 and 0.5 mA cm^{-2}. The period of each striping or plating was set as 0.5 h, which corresponds to the area-specific capacity of 0.15 and 0.25 mAh cm^{-2}. As shown in Figure 4e, the Li/LLZTO-S/Li symmetric cell maintains steadily for 1000 h with the consistent overpotential of 21 mV at the current density of 0.3 mA cm^{-2}. Moreover, the steady overpotential is also achieved at the current density of 0.5 mA cm^{-2} for 600 h, which displays a small voltage hysteresis of ≈47 mV, Figure 4f. The prolonged stable cycling of the symmetric cells emphasizes the great transport property across the Li/LLZTO-S interface.

The hybrid solid-state Li/$LiFePO_4$ full cell was constructed with the LLZTO-S electrolyte pellet. The cathode/electrolyte interface was wetted by a tiny amount of liquid organic electrolyte (1.0 M $LiPF_6$ in EC:DMC:EMC = 1:1:1 vol%, ≈10 μL), as graphically shown in **Figure** 5a. The initial charge and discharge specific capacities of the full cell are 152.7 and 138.5 mA h g^{-1} at a current density of 30 μA cm^{-2}, respectively, delivering a coulombic efficiency of 90.7%. The charge and discharge specific capacity of the full cell matins 140.5 and 133 mA h g^{-1} after 100 times cycling, showing a good stable performance, Figure 5b. The detail curves for 1st, 50th, and 100th are shown in Figure 5c, indicating the stable charge-discharge platform. In addition, to

obtain a more stable cathode/LLZO interface at high current densities, the incorporation of a tiny amount of liquid organic electrolyte was further optimized (1.0 M $LiPF_6$ in EC: DEC = 1:1 vol%, ≈10 µL). As shown in Figure 5d, the rate performance of the full cell was tested with the step-increased current densities at 50, 100, 150, 300, and 450 µA cm^{-2}. The corresponding discharge capacities are 149.2, 139.4, 138.2, 118.8, and 99.4 mA h g^{-1}. After high-rate cycle testing, the cell recovers to a discharge capacity of 150.1 mA h g^{-1} at 50 µA cm^{-2}, showing great stability and reversibility compared with the reported work (Table S1, Supporting Information).

3. Conclusion

In summary, a lithiophilic garnet pellet is achieved by physically decreasing the pellet surface roughness without the need to fully remove the well-known lithiophobic Li_2CO_3 on the surface. The smooth garnet pellet has a tight and seamless contact with lithium metal. Importantly, the pure Li_2CO_3 pellets with low surface roughness can also be easily wetted by lithium metal. Meanwhile, the smooth garnet pellet possesses a smaller actual area, which leads to a slower reaction rate to air and displays improved air stability. Without further interfacial design, the assembled symmetric cell with smooth LLZTO pellet shows ultralow interfacial resistance (≈2 Ohm cm^2) and high critical current density (1.4 mA cm^{-2}). Moreover, the symmetric cell assembled with a smooth but partially scratched pellet displays degraded electrochemical performance. This unambiguously points toward the importance of controlling the roughness of the electrolyte surface. We believe our work will help in understanding the interface engineering of Li/SSEs and promote the development of ASSLBs.

Supporting Information

Supporting Information is available from the Wiley Online Library or from the author.

Acknowledgements

J.Z. and C.W. contributed equally to this work. The authors would like to acknowledge the financial support from the National Natural Science Foundation of China (Grant No. 11804261), the National Key Research and Development Program of China (Grant No. 2019YFA0704900), the Postdoctoral Innovation Talent Support Program (Grant No. BX20240175), and the China Postdoctoral Science Foundation (Grant No. 2024M751549).

Conflict of Interest

The authors declare no conflict of interest.

Data Availability Statement

The data that support the findings of this study are available from the corresponding author upon reasonable request.

Keywords

garnet electrolytes, Li_2CO_3, solid-state batteries, surface roughness

Received: September 1, 2024
Revised: October 23, 2024
Published online:

[1] J. M. Tarascon, M. Armand, *Nature* **2001**, *414*, 359.
[2] L. Trahey, F. R. Brushett, N. P. Balsara, G. Ceder, L. Cheng, Y.-M. Chiang, N. T. Hahn, B. J. Ingram, S. D. Minteer, J. S. Moore, K. T. Mueller, L. F. Nazar, K. A. Persson, D. J. Siegel, K. Xu, K. R. Zavadil, V. Srinivasan, G. W. Crabtree, *Proc. Natl. Acad. Sci. USA* **2020**, *117*, 12550.
[3] L. Wen, X. Wang, G. Q. Liu, H. Z. Luo, J. Liang, S. X. Dou, *Surf. Innovations* **2017**, *6*, 13.
[4] J. Janek, W. G. Zeier, *Nat. Energy* **2016**, *1*, 16141.
[5] X.-B. Cheng, R. Zhang, C.-Z. Zhao, Q. Zhang, *Chem. Rev.* **2017**, *117*, 10403.
[6] V. Thangadurai, H. Kaack, W. J. F. Weppner, *J. Am. Ceram. Soc.* **2003**, *86*, 437.
[7] Z. H. Zhang, T. Wei, J. H. Lu, Q. M. Xiong, Y. H. Ji, Z. Y. Zhu, L. T. Zhang, *Int. J. Miner., Metall. Mater.* **2021**, *28*, 1565.
[8] Z. Jiang, S. Wang, X. Chen, W. Yang, X. Yao, X. Hu, Q. Han, H. Wang, *Adv. Mater.* **2020**, *32*, 1906221.
[9] C. Wang, J. Liang, Y. Zhao, M. Zheng, X. Li, X. Sun, *Energy Environ. Sci.* **2021**, *14*, 2577.
[10] P. Lu, D. Wu, L. Chen, H. Li, F. Wu, *Electrochem. Energy Rev.* **2022**, *5*, 3.
[11] J. Wu, S. Liu, F. Han, X. Yao, C. Wang, *Adv. Mater.* **2021**, *33*, 2000751.
[12] C. Wang, J. Liang, J. T. Kim, X. Sun, *Sci. Adv.* **2022**, *8*, eadc9516.
[13] X. Li, J. Liang, X. Yang, K. R. Adair, C. Wang, F. Zhao, X. Sun, *Energy Environ. Sci.* **2020**, *13*, 1429.
[14] K.-H. Park, K. Kaup, A. Assoud, Q. Zhang, X. Wu, L. F. Nazar, *ACS Energy Lett.* **2020**, *5*, 533.
[15] S.-J. Tan, X.-X. Zeng, Q. Ma, X.-W. Wu, Y.-G. Guo, *Electrochem. Energy Rev.* **2018**, *1*, 113.
[16] M. Xin, X. Lian, X. Gao, P. Xu, W. Li, F. Dong, A. Zhang, H. Xie, Y. Liu, *J. Colloid Interface Sci.* **2022**, *629*, 980.
[17] M. Wu, J. Song, X. Zhu, H. Zhan, T. Tian, R. Wang, J. Lei, H. Tang, *Sci. China Mater.* **2022**, *66*, 522.
[18] J. A. Isaac, D. Devaux, R. Bouchet, *Nat. Mater.* **2022**, *21*, 1412.
[19] Y. S. Park, J. M. Lee, E. J. Yi, J. W. Moon, H. Hwang, *Materials* **2021**, *14*, 10.
[20] G. Y. Tian, H. Li, B. Khalid, Z. J. Zhao, *Chem. Eng. J.* **2022**, *430*, 132803.
[21] V. Thangadurai, S. Narayanan, D. Pinzaru, *Chem. Soc. Rev.* **2014**, *43*, 4714.
[22] N. Zhao, W. Khokhar, Z. Bi, C. Shi, X. Guo, L.-Z. Fan, C.-W. Nan, *Joule* **2019**, *3*, 1190.
[23] S. Abouali, C. H. Yim, A. Merati, Y. Abu-Lebdeh, V. Thangadurai, *ACS Energy Lett.* **2021**, *6*, 1920.
[24] J. Wang, G. Huang, X. B. Zhang, *Batteries Supercaps* **2020**, *3*, 1006.
[25] H. Huo, J. Luo, V. Thangadurai, X. Guo, C.-W. Nan, X. Sun, *ACS Energy Lett.* **2020**, *5*, 252.
[26] X. Han, Y. Gong, K. K. Fu, X. He, G. T. Hitz, J. Dai, A. Pearse, B. Liu, H. Wang, G. Rubloff, *Nat. Mater.* **2016**, *16*, 572.
[27] C. W. Wang, Y. H. Gong, B. Y. Liu, K. Fu, Y. G. Yao, E. Hitz, Y. J. Li, J. Q. Dai, S. M. Xu, W. Luo, E. D. Wachsman, L. B. Hu, *Nano Lett.* **2017**, *17*, 565.
[28] C. Chen, Q. Li, Y. Q. Li, Z. H. Cui, X. X. Guo, H. Li, *ACS Appl. Mater. Interfaces* **2018**, *10*, 2185.
[29] H. Y. Huo, Y. Chen, R. Y. Li, N. Zhao, J. Luo, J. G. P. da Silva, R. Mucke, P. Kaghazchi, X. X. Guo, X. L. Sun, *Energy Environ. Sci.* **2020**, *13*, 127.
[30] H. Duan, W. P. Chen, M. Fan, W. P. Wang, L. Yu, S. J. Tan, X. Chen, Q. Zhang, S. Xin, L. J. Wan, Y. G. Guo, *Angew. Chem., Int. Ed.* **2020**, *59*, 12069.

[31] M. Motoyama, Y. Tanaka, T. Yamamoto, N. Tsuchimine, S. Kobayashi, Y. Iriyama, *ACS Appl. Energy Mater.* **2019**, *2*, 6720.
[32] C. W. Wang, H. Xie, W. W. Ping, J. Q. Dai, G. L. Feng, Y. G. Yao, S. M. He, J. Weaver, H. Wang, K. Gaskell, L. B. Hu, *Energy Storage Mater.* **2019**, *17*, 234.
[33] Z. Qin, Y. Xie, X. Meng, D. Qian, C. Shan, D. Mao, G. He, Z. Zheng, L. Wan, Y. Huang, *Chem. Eng. J.* **2022**, *447*, 137538.
[34] A. Sharafi, E. Kazyak, A. L. Davis, S. Yu, T. Thompson, D. J. Siegel, N. P. Dasgupta, J. Sakamoto, *Chem. Mater.* **2017**, *29*, 7961.
[35] F. M. Pesci, A. Bertei, R. H. Brugge, S. P. Emge, A. K. O. Hekselman, L. E. Marbella, C. P. Grey, A. Aguadero, *ACS Appl. Mater. Interfaces* **2020**, *12*, 32806.
[36] S. A. Pervez, B. P. Vinayan, M. A. Cambaz, G. Melinte, T. Diemant, T. Braun, G. Karkera, R. J. Behm, M. Fichtner, *J. Mater. Chem. A* **2020**, *8*, 16451.
[37] L. Cheng, E. J. Crumlin, W. Chen, R. Qiao, H. Hou, S. F. Lux, V. Zorba, R. Russo, R. Kostecki, Z. Liu, *Phys. Chem. Chem. Phys.* **2014**, *16*, 18294.
[38] Q. Wang, G. Yu, B. Luo, W. Ji, Z. Liu, M. Li, Y. Nong, Y. Tian, X. Wang, J. Zhang, C.-L. Chen, C.-K. Chang, Z. Sang, Z. Zhao, R. Zhao, J. Liang, *ACS Nano* **2024**, *18*, 18622.
[39] R. Pfenninger, M. Struzik, I. Garbayo, E. Stilp, J. L. Rupp, *Nat. Energy* **2019**, *4*, 475.
[40] H. Y. Huo, Y. Chen, N. Zhao, X. T. Lin, J. Luo, X. F. Yang, Y. L. Liu, X. X. Guo, X. L. Sun, *Nano Energy* **2019**, *61*, 119.
[41] R. N. Wenzel, *J. Phy. Chem.* **1949**, *53*, 1466.
[42] B. Yin, Z. Qiao, C. Liu, *Mater. Des.* **2016**, *106*, 226.
[43] R. Freitas, E. J. Reed, *Nat. Commun.* **2020**, *11*, 3260.
[44] W. Ji, B. Luo, Q. Wang, G. Yu, Z. Liu, Z. Zhao, R. Zhao, S. Wang, X. Wang, B. Zhang, J. Zhang, F. Hou, J. Liang, *Adv. Energy Mater.* **2023**, *13*, 2300165.
[45] T. Krauskopf, B. Mogwitz, H. Hartmann, D. K. Singh, W. G. Zeier, J. Janek, *Adv. Energy Mater.* **2020**, *10*, 2000945.
[46] X. Yao, X. Lu, Y. Zhou, T. Šamořil, J. Bi, M. G. Masteghin, H. Zhang, L. Askew, J. Kim, F. Xiong, J. Wang, D. C. Cox, T. Sui, I. Gilmore, S. R. P. Silva, L. Mai, G. Hinds, P. R. Shearing, J. Park, Y. Zhao, *Energy Environ. Sci.* **2023**, *16*, 2167.
[47] Y. Wu, K. Wang, K. Liu, Y. Long, C. Yang, H. Zhang, W. Pan, W. Si, H. Wu, *Adv. Energy Mater.* **2023**, *13*, 2300809.
[48] B. Zhao, W. C. Ma, B. B. Li, X. T. Hu, S. Y. Lu, X. Y. Liu, Y. Jiang, J. J. Zhang, *Nano Energy* **2022**, *91*, 106643.
[49] J. X. Zhang, R. H. Yu, J. Li, H. Y. Zhai, G. J. Tan, X. F. Tang, *Energy Environ. Mater.* **2022**, *5*, 962.
[50] Y. Niu, Z. Yu, Y. Zhou, J. Tang, M. Li, Z. Zhuang, Y. Yang, X. Huang, B. Tian, *Nano Res.* **2022**, *15*, 7180.
[51] X. N. Ma, Y. L. Xu, *ACS Appl. Mater. Interfaces* **2022**, *14*, 2939.
[52] A. Baniya, A. Gurung, J. Pokharel, K. Chen, R. Pathak, B. S. Lamsal, N. Ghimire, R. S. Bobba, S. I. Rahman, S. Mabrouk, A. L. Smirnova, K. Xu, Q. Qiao, *ACS Appl. Energy Mater.* **2022**, *5*, 648.
[53] R. Xu, F. Liu, Y. Ye, H. Chen, R. R. Yang, Y. Ma, W. Huang, J. Wan, Y. Cui, *Adv. Mater.* **2021**, *33*, 2104009.
[54] F. Okur, H. Zhang, D. T. Karabay, K. Muench, A. Parrilli, A. Neels, W. Dachraoui, M. D. Rossell, C. Cancellieri, L. P. H. Jeurgens, K. V. Kravchyk, M. V. Kovalenko, *Adv. Energy Mater.* **2023**, *13*, 2203509.